Linearized fluctuating hydrodynamics via random polynomials

Farid Taghinavaz[1,*] and Giorgio Torrieri[2,†]

[1]*School of Particles and Accelerators, Institute for Research in Fundamental Sciences (IPM), P.O. Box 19395-5531, Tehran, Iran*

[2]*Universidade Estadual de Campinas (Unicamp), R. Sérgio Buarque de Holanda, 777, Campinas 13083-859, Brazil*

(Received 8 August 2024; accepted 21 August 2024; published 11 September 2024)

We argue that an ensemble of backgrounds best describes hydrodynamic dispersion relations in a medium with few degrees of freedom and is therefore subject to strong thermal fluctuations. In the linearized regime, dispersion relations become describable by polynomials with random coefficients. We give a short review of this topic and perform a numerical study of the distribution of the roots of polynomials whose coefficients are of the order of a Knudsen series but fluctuate in accordance with canonical fluctuations of temperature. We find that, remarkably, the analytic structure of the poles of fluctuating dispersion relations is very different from deterministic ones, particularly regarding the distribution of imaginary parts with respect to real components. We argue that this provides evidence that hydrodynamic behavior persists, and is enhanced, by nonperturbative background fluctuations.

DOI: 10.1103/PhysRevD.110.056019

I. PHYSICAL MOTIVATION

The effect of thermal fluctuations in hydrodynamics is still not understood fundamentally and is of great phenomenological interest due to the seeming applicability of hydrodynamics in small systems [1], which contradicts naive fluctuation-dissipation thinking, where the mean free path l_{mfp} (a function of viscosity η as well as entropy density s and temperature T, related to the microscopic relaxation time τ_π) is straightforwardly related to the fluctuation scale l_{fluct} (a function, in the absence of conserved charges, of only the equilibrium temperature T, which, for a relativistic system, also reflects the number of degrees of freedom N per unit volume V via the degeneracy g [2,3]),

$$l_{mfp} \sim \frac{\eta}{sT} \sim \tau_\pi \sim l_{\text{fluct}} \sim C_V T^2 \sim \underbrace{\frac{1}{gT}}_{gT^3 \sim N/V}. \tag{1}$$

Small system hydrodynamics [1] puts into doubt this $l_{mfp} \sim l_{\text{fluct}}$ scaling, especially since emergence of "collective" behavior in systems with very few degrees of freedom has also been reported in other situations, such as ultracold atoms [4] and even everyday objects (the "Brazil nut effect" [5]). These findings, at very different energy scales, show that perhaps the way we think about collectivity (where first we take the "many particle limit" and then the "small mean free path limit" [3,6]) needs to be rethought.

One way the hierarchy in Eq. (1) could fail [7] is the realization that hydrodynamic degrees of freedom [flow u_μ, heat current Q_μ, temperature T, chemical potentials μ which go into pressure and energy (p, ε) as well as dissipative tensor $\Pi_{\mu\nu}$] do not match with the observable quantities (energy-momentum tensor current $T_{\mu\nu}$ and conserved current J_μ). Furthermore, while the latter is specific to each element of the ensemble and extensive, $\beta_\mu = u_\mu/T$, μ are considered in the grand canonical limit to be Lagrange multipliers, intensive in the thermodynamic limit.

This suggests that once one applies statistical mechanics limits (ergodicity or each microstate is equally likely [8]) to each cell but allows fluctuations, redundances will appear where each microstate will have a multiplicity of descriptions, not unlike gauge configurations and ghosts in a quantum field [7]. What an observer interprets as u_μ in some Landau prescription will be interpreted as heat flow Q_μ by another observer using the Eckart prescription or $\Pi_{\mu\nu}$ in the Müller-Israel-Stewart (MIS) prescription. The important fact is that, since these are multiple descriptions of the same system, the dynamics when fluctuations are included should be invariant with respect to such choices, just like the dynamics of a gauge theory is gauge independent. These have the potential to drastically alter

*Contact author: ftaghinavaz@ipm.ir
†Contact author: torrieri@ifi.unicamp.br

the applicability of hydrodynamics as a function of the number of participants.

While a quantitative understanding of this idea is very involved and elusive, we can make some simple considerations using sound dispersion relations: Let us think of a sound wave perturbation propagating in a background subject to thermodynamic fluctuations. If $l_{mfp} \gg l_{\rm fluct}$ one can think of the fluctuation as being a localized random perturbation within the sound wave. We then recover the usual fluctuation-dissipation relations of [2]. But if $l_{mfp} \leq l_{\rm fluct}$ then the background properties (viscosity, speed of sound, etc.) fluctuate while the perturbations propagate. One can then think of the coefficients of that sound mode to be random numbers, whose distribution is given by statistical mechanics.

The consequences of this can be nontrivial: We know that a pole on the real axis, related to the existence of a real solution, indicates a wave propagating asymptotically. A pole on the imaginary axis indicates a "nonhydrodynamic mode," and a branch cut suggests a violation of (global) univalence, which transits between these regimes. As we will show, the relation between the distribution of these objects to the distribution of coefficients is rich and nontrivial, indicating that the fluctuating regime is indeed far from a trivial extrapolation of the deterministic one.

To explain these points further, the best interpretation of the dispersion relations is the following Gedanken experiment: let an experimentalist have access to a large ensemble of field configurations of $T_{\mu\nu}(x,t)$ [i.e., many "events" where $T_{\mu\nu}(x,t)$ is measured over a fine lattice in (x,t)]. One can then take the average over a single event (denoted $\langle\ldots\rangle$; this can be done by histogramming in bins of $x-x', t-t'$ sampled in a single event) or over the whole ensemble of events (denoted $\{\ldots\}$). This can be done by the usual technique of defining an event specific system of coordinates around the event's center of mass and origin x_0, t_0 and building histograms in bins of $x-x_0, t-t_0$ across events. In the ensemble average limit (where the Boltzmann equation and molecular chaos apply or, in general, where the number of degrees of freedom is effectively infinite) $\{\langle\ldots\rangle\} \simeq \langle\{\ldots\}\rangle$ but we will look at deviations from that limit where there is enough statistics to do $\langle\ldots\rangle$ within a single event.

Thus, let us measure its two-point function $\langle T_{\mu\nu}(x,t)T_{\mu\nu}(x',t')\rangle$ event by event, take a fast Fourier transformation event by event, and infer, still event by event, a $\omega = c_n k^n$ to the fast Fourier transform, yielding an ensemble $\{c_n\}$ over all events. One can do this via a fitting process if the event is large enough or by expressing larger cumulants $\langle T_{\mu\nu}(x_i,t_i)\ldots T_{\mu\nu}(x_1,t_1)\rangle$ in terms of two-point functions $\langle T_{\mu\nu}(x_i,t_i)T_{\mu\nu}(x_{i+1},t_{i+1})\rangle$, in analogy as to what is done with azimuthal angles to measure flow in small systems [9].

In the limit where thermal fluctuations are smaller in scale with respect to the mean free path, one should obtain the Kubo formula [see Sec. II, Eq. (8) for $m=1$] where, because of the $\lim_{k\to 0} k^{-1}\ldots$ limit, only the infrared part of fluctuations contributes to the dynamics (in other words, thermal fluctuations are "local" with respect to gradients and the mean free path, as also argued in [7,8,10]). In the opposite limit, one can think of the perturbation propagating inside a thermal fluctuation. As we shall argue toward the end of Sec. II c_n's fluctuate independently according to the whole spectral function of $\langle\tilde{T}_{\mu\nu}(\omega,k)\tilde{T}_{\mu\nu}(\omega',k')\rangle$ (nonhydrodynamic modes and all) [11]. The experimentalist then uses that information, to understand its further dynamics, by extracting the hydrodynamic parameters in each event ($\{e,p\}, \{\eta/s\}$ and so on) and using them as an effective field theory expansion in the Knudsen number to predict the subsequent evolution of an initial perturbation in that given event via a propagator [which we define in Eq. (6)], constructed for that event (we, of course, assume the experimentalist can also construct perturbations in that event and there are enough degrees of freedom to construct such a perturbation).

It is immediately evident from the mathematics literature [12,13] how fluctuations affect this conclusion. As $m \to \infty$ in Eq. (2) and in the limit that $\eta/s \sim 1$ it is a classic result [14] that the roots converge to a circle in the complex plane. As a result,

The fraction of real roots approaches 0.

The probability of having *at least one root* approaches 1. This means that, in events where Eq. (2) has real roots for Fourier coefficients corresponding to the initial spacial distribution, that perturbation will propagate asymptotically in the linear regime. In events where the root has an imaginary part, that perturbation will propagate to a scale proportional to the imaginary part (which is large for that perturbation to be "hydrodynamic").

In the next section, we will examine more closely what the dispersion relation described in this section looks like, and in the rest of the work, we proceed with a numerical study of it.

II. DISPERSION RELATIONS IN A FLUCTUATING MEDIUM

Let us therefore consider a perturbation with a general dispersion relation. Neglecting chemical potential, dimensionality, and the spacetime structure of the dispersion relation forces us into [15–17]

$$\omega^{\pm}(k) = -i\sum_{n=1}^{m} c_n^{\pm} k^n, \qquad c_n^{\pm} = e^{\pm\frac{in\pi}{2}}\mathcal{O}\left(c_s^n\left(\frac{\eta}{s}\right)^{n-1}\right)\tau_{\rm micro}^{n-1},$$
$$\tau_{\rm micro} \sim \frac{1}{T}, \tag{2}$$

where c_s is the speed of sound in that medium. For example, the usual Navier-Stokes dispersion relation is described by

$$c_1 = c_s, \qquad c_2 = \mathcal{O}(1)\frac{\eta}{s}\tau. \tag{3}$$

We note that we put together Eqs. (7) and (8) of [15] because event by event and with a finite space resolution the "sound" and "diffusion" modes can only be distinguished on a Bayesian basis. The "complex phase" dependence on "n" is then determined by analyticity [16] where $g \sim N$ is the microscopic degeneracy and N is the number of particles. Note that the first real coefficient does not fluctuate in this simplified model because $c_s^2 = 1/3$.

It is well known that, for a system with N particles (for a small system this can be interpreted as the multiplicity), temperature fluctuations are given by

$$\langle (\Delta T)^2 \rangle = \frac{2T^2}{N c_v}, \tag{4}$$

where cv is the heat capacity at constant volume per each degree of freedom. (see [18] and references therein). Note that, since the multiplicity is observable, we prefer to write the fluctuation in terms of the multiplicity rather than the degeneracy as in Eq. (1), where c_v is the heat capacity at constant volume per each degree of freedom.[1]

It is therefore natural to assume temperature to fluctuate with a Gaussian or a Poissonian distribution given by a width of the order shown in Eq. (4) and c_n to fluctuate in response,

$$\langle (\Delta c_n)^2 \rangle \sim \frac{\mathcal{O}(c_s^n (\frac{\eta}{s})^{n-1})}{N c_v} \langle (T)^{-2(n-1)} \rangle. \tag{5}$$

Using the terminology prevalent in the literature, if one has a current correlator defined by

$$J(\Delta t, \Delta x) = \int d^3k \frac{\exp\left[i(\omega^{\pm}(k)\Delta t - k\Delta x)\right]}{\omega^{\pm}(k) + i\sum_{n=1}^{m} c_n^{\pm} k^n}, \tag{6}$$

a hydrodynamic mode propagates to $\Delta x \to \infty$ and a nonhydrodynamic mode to a finite Δx (with a long-lived nonhydrodynamic mode propagating for $\Delta t \to \infty$). The existence of nonhydrodynamic poles and branch cuts in $J = \langle T_{ij}(x), T_{ij}(x') \rangle$ has been a topic of recent interest [11] with recent claims [19–22] using a relaxation Boltzmann equation (where fluctuations are not included) pointing to long-lived nonhydrodynamic modes.

Thus, naively, if one neglects fluctuations, nonhydrodynamic modes dominate. However, as $\Delta x \to \infty$ in Eq. (6) isolates real roots a hydrodynamic mode will always emerge, rendering any nonhydrodynamic mode irrelevant.

Note that according to the ergodic picture of statistical mechanics [8] fluctuation scaling of c_n is independent of the choice of hydrodynamic frame. Hence, it should not by default be associated with any "model" of hydrodynamics. The specific transport coefficients of Landau, Eckart, Israel-Stewart, and other models will *not* be random fluctuating quantities c_n themselves but rather will be a Bayesian inference of the coefficients c_n and their relationships [7].

This might prove confusing to someone who develops a hydrodynamic effective field theory from a thermostatic frame and an "objective" definition of u_μ (that is, most of the literature). This is an important point as it also leads to the ansatz assumed here, where c_n's fluctuate *independently* rather than follow fluctuations of T and N, as expected from the fact that the average values of c_n would be functions of these two parameters.

We note that every c_n in Eq. (2) comes from a different degree of freedom, something clear from both effective [3] and transport [23] theory. The dispersion relation whose zeros are represented by Eq. (2) is directly derivable from an eigenvalue equation of a characteristic matrix of correlators

$$\det |H_n \times H_{0m} - k I_{nm}| = 0, \tag{7}$$

where the term H_n is given by a generalized Kubo formula

$$H_n \propto \lim_{k\to 0} \frac{1}{k^n} \frac{d^n}{dk^n} \int e^{ikx} dx \langle T_{ij}(x) T_{ij}(0) \rangle \tag{8}$$

[in [3] these coefficients are denoted by $X_{I_1 \ldots I_n}$, in [23] by moments of $f(x, p)$] as well as an initial gradient H_{0m}. Given that each derivative will be a highly nontrivial function of microscopic physics and initial conditions, representing these matrix coefficients by random numbers is a consequence of local equilibrium dynamics being dominated by fluctuation-dissipation relations. Physically, thermal fluctuations continuously produce sound waves, which interact and deform the background according to the Feynman rules developed. For instance, in [24] we now "renormalize the background" with these sound waves, using methods in [2,6] and introduce a fluctuation on top of that [the driven fluctuation in Eq. (6)]. Thus, the independent random coefficients of the dispersion relation reflect the fact that, when the sampling is insufficient to reconstruct the phase space distribution, the problem of thermalization can be connected to a random matrix problem [10].

In fact, if one thinks of hydrodynamics as a limit of the Boltzmann equation, small systems can be thought of as promoting phase space functions $f(x, p)$ to functionals [10,25,26] then terms of the dispersion relation of $\mathcal{O}(k^n)$ become related [23] to the probability distribution of the nth moment of p of the functional distribution of the perturbation $\delta f(x, p)$, which leads to the sort of random polynomial we examine.

In the conformal case, the absence of intrinsic scales beyond energy/temperature forces the scaling of fluctuations of Eq. (5) when $\eta/(sT)$ is such that the fluctuation

[1] In a theory with a varying number of degrees of freedom, this represents the microscopic degeneracy, e.g., $\sim N_c^2$ for a 't Hooft type model.

domain is of the order of the sound wave propagation domain.[2]

A basic question in that context is "Will this disturbance propagate, far in the IR?" The probability of a disturbance of $T_{\mu\nu}$ to propagate long distance is therefore represented by the probability of finding a real root in some element of the ensemble, rather than some parameter depending on the choice for the thermostatic frame (something inferred from the ensemble as much as any other observation).

While the study of random polynomials is a developed field of pure mathematics (we give a short overview in the Appendix), as far as we know no analytical results exist which are directly relevant to the type of polynomials described in this section. In this work, we shall proceed numerically. In Sec. III, we review the MIS formalism and derive the low-lying sound mode equation, which we compare with the random modes solutions provided in Sec. IV. Eventually, we give a comprehensive conclusion with an outlook for future studies.

III. REVIEW OF MIS FORMALISM

By the MIS model, we address an uncharged conformal system characterized by the following constitutive relation:

$$T^{\mu\nu} = \varepsilon u^\mu u^\nu - p\Delta^{\mu\nu} + \Pi^{\mu\nu}, \tag{9}$$

where $\Pi^{\mu\nu} = -2\eta\sigma^{\mu\nu}$ with η denoting the shear viscosity and $\sigma^{\mu\nu} = \frac{1}{2}(\nabla^\mu u^\nu + \nabla^\nu u^\mu - \frac{2}{3}\Delta^{\mu\nu}\nabla\cdot u)$ represents the shear-stress tensor and $\nabla_\mu = \Delta_{\mu\nu}\partial^\nu$. The governing dynamical equations are given by [27]

$$\begin{aligned} \partial_\mu T^{\mu\nu} &= 0, \\ \tau u^\nu \partial_\nu \Pi^{\mu\nu} + \Pi^{\mu\nu} &= -2\eta\sigma^{\mu\nu}, \end{aligned} \tag{10}$$

where τ is the relaxation time associated with $\Pi^{\mu\nu}$ approaching its on-shell value, $-2\eta\sigma^{\mu\nu}$. $\Pi^{\mu\nu}$ is a regulator field with the lifetime τ, being the first nonconserved operator in the nonhydrodynamic spectrum. Our analysis focuses on the sound channel in which, by solving Eq. (10) for small perturbations, the equation takes the following form [27]:

$$\omega^3 + \frac{i\omega^2}{\tau} - \left(c_s^2 + \frac{\gamma_s}{w\tau}\right)\omega k_z^2 - \frac{ic_s^2 k_z^2}{\tau} = 0, \tag{11}$$

[2]Actually, a full model would contain not just the Legendre transform/Lagrange multiplier for energy T but also of 4-momentum, $\beta_\mu = u_\mu/T$. As argued in the Introduction and [7], the full fluctuating dynamics will be affected by the redundances implicit in the freedom to reparametrize the spacetime foliation whose structure, analogous to Faddeev-Popov ghosts in Gauge theory, is highly nontrivial. In this work, we concentrate only on the effect of these redundances on linearized dispersion relations, parametrized by c_n.

where $c_s^2 = \partial\varepsilon/\partial p$ is the speed of sound, $\gamma_s = 4\eta/3$, and $w = \varepsilon + p$ is enthalpy. We can make the substitutions

$$\omega = i\frac{\beta}{\tau}, \qquad k_z^2 \equiv z = \frac{\tilde{z}}{c_s^2\tau^2}, \qquad X \equiv -1 + \frac{\gamma_s}{8c_s^2\tau w}, \tag{12}$$

resulting in the following dispersion relation:

$$\beta^3 + \beta^2 + \tilde{z}\beta(9 + 8X) + \tilde{z} = 0. \tag{13}$$

In what follows, as a part of the computation, we want to compare the random modes structure with the infrared (IR) solutions of Eq. (13).

IV. ALGORITHM TO FIND THE PROBABILITY OF PROPAGATING MODES

In our calculations, we utilize the assumption of conformal symmetry, which implies that $\partial p/\partial\varepsilon = c_s^2 = 1/3$. Furthermore, we scale the frequency "ω" by the temperature, denoted as "T." We aim to calculate the probability of propagation for real modes within the IR limit of the MIS theory. We perform this analysis for two specific sets of parameters: (i) $\tau_1 T = (2 - \ln 2)/(2\pi)$, which corresponds to the $\mathcal{N} = 4$ result [28], and (ii) $\tau_2 T = 0.1/(2\pi)$. We investigate the behavior at both high and low momenta for each parameter set. We examine each case using series expansions of order 4 and order 10 in momentum to assess the influence of series order on our findings. Here, we outline the steps followed in our analysis.

(1) We generate the modes using the following series [15–17]:

$$\omega_s(k) = -i\sum_{n=1}^{s} c_n e^{i\frac{n\pi}{2}} k^n - i\sum_{n=1}^{\frac{s}{2}} d_{2n} k^{2n}. \tag{14}$$

The choice of this series is due to the mathematical properties of dispersion relation at low momenta which we assume to be free of any singular characters like branch point, branch cut, etc. Indeed, the series in Eq. (14) generates the sound and the diffusive channel because, in an experimental setup, we cannot separate these channels. Based on the dimensionality and spacetime structure of each mode, the c_n and d_n coefficients must take the following form:

$$(c_n, d_n) = (a_n, b_n) \times c_s^n \left(\frac{\eta}{s}\right)^{n-1} \tau^{n-1}. \tag{15}$$

The coefficients (a_i, b_i) are fluctuating numbers corresponding to the first (second) term on the rhs of Eq. (14). These fluctuations are essentially thermal fluctuations because they are dimensionful quantities. In a conformal theory (which we take

here) with only one scale, such as temperature, any dimensionful fluctuation can be converted into thermal fluctuation.

(2) For our later purpose, we need the fourth and tenth expansion of Eq. (14). In fourth order, this series takes the following form:

$$\omega_4(k) = a_1 c_s k + i(a_2 - b_2)\frac{\eta}{s}\tau c_s^2 k^2 - a_3\left(\frac{\eta}{s}\right)^2 \tau^2 c_s^3 k^3 - i(a_4 + b_4)\left(\frac{\eta}{s}\right)^3 \tau^3 c_s^4 k^4 + \mathcal{O}(k^5). \quad (16)$$

For order 10, it becomes

$$\begin{aligned}\omega_{10}(k) = {} & a_1 c_s k + i(a_2 - b_2)\frac{\eta}{s}\tau c_s^2 k^2 - a_3\left(\frac{\eta}{s}\right)^2 \tau^2 c_s^3 k^3 \\ & - i(a_4 + b_4)\left(\frac{\eta}{s}\right)^3 \tau^3 c_s^4 k^4 + a_5\left(\frac{\eta}{s}\right)^4 \tau^4 c_s^5 k^5 \\ & + i(a_6 - b_6)\left(\frac{\eta}{s}\right)^5 \tau^5 c_s^6 k^6 - a_7\left(\frac{\eta}{s}\right)^6 \tau^6 c_s^7 k^7 \\ & - i(a_8 + b_8)\left(\frac{\eta}{s}\right)^7 \tau^7 c_s^8 k^8 + a_9\left(\frac{\eta}{s}\right)^8 \tau^8 c_s^9 k^9 \\ & + i(a_{10} - b_{10})\left(\frac{\eta}{s}\right)^9 \tau^9 c_s^{10} k^{10}. \end{aligned} \quad (17)$$

It is worth mentioning that each term in the series mentioned above fluctuates independently, as they originate from the corresponding n-point functions of $T_{\mu\nu}$. We take $\eta/s = 1/(4\pi)$ in our numerical setup.

(3) We employ a discretization of $k = 4\pi T m/1000$ for our analysis. For low-momentum (LM) results, the algorithm is applied to $m = [1,2,\ldots,100]$, and for high-momentum (HM) it runs for $m = [300,301,\ldots,500]$. We take each momentum bin independent of its neighbors, similar to a random walk.

(4) The only parameter characterizing the background is temperature (no conserved charges) whose extensive lagrange multiplier is the temperature. The variation of other thermodynamic quantities therefore depends on the variation of temperature [29] as well as the number of degrees of freedom of the system N. The temperature distribution follows a Gaussian distribution with the deviation provided in Eq. (4). We assume $c_v = g$, where g represents the degrees of freedom. We set $g = 6$, accounting for three momentum directions and three for spatial displacements. Given that all terms are proportional to T and are positive, we can adopt the following distribution for random and dimensionless (a_n, b_n) numbers:

$$\mathcal{D}(N,x) = \frac{1}{2}\sqrt{\frac{gN}{\pi}}\frac{e^{-\frac{gN}{4}(x-1)^2}}{1 - \frac{\mathrm{Erf}\left(\frac{\sqrt{gN}}{2}\right)}{2}}, \quad x \geq 0, \quad (18)$$

where N counts the number of particles, and $\mathrm{Erf}(x) = \frac{2}{\sqrt{\pi}}\int_0^x e^{-t^2} dt$ is the error function used to normalize the distribution.

(5) In each momentum bin, we generate 10^5 results, with the random coefficients selected according to the distribution equation (18). After generating the series as given in Eq. (16) or Eq. (17), we obtain their real and imaginary parts, enabling us to analyze them in various ways.

(6) After obtaining the distribution of roots in each momentum bin, we fit the distribution of either the real or imaginary parts to a Gaussian distribution of the form

$$\mathcal{D}_G(x_{0_m}, \sigma_m; x) = \frac{1}{\sqrt{2\pi\sigma_m^2}} e^{-\frac{(x-x_{0_m})^2}{2\sigma_m^2}}, \quad (19)$$

to get the optimal mean x_{0_m} and standard deviation σ_m^2. The quality of the propagating modes is evaluated by the ratio $x_{0_m}^{\mathrm{Im}}/x_{0_m}^{\mathrm{Re}}$. Modes with a smaller ratio deserve to be better propagating modes.

(7) Some parts of our results are devoted to comparing the generated series with hydrosolutions or the low momentum expansion of solutions of Eq. (13). For $\eta/s = 1/(4\pi)$ and $c_s^2 = 1/3$, the order 4 series becomes

$$\begin{aligned}\Omega_{1,2}^{(4)}(k) = {} & \pm\left(\frac{k}{\sqrt{3}} + \frac{k^3}{24\sqrt{3}\pi^2 T^2}(-1 + 4\pi T\tau)\right) \\ & - \frac{ik^2}{6\pi T} - \frac{ik^4\tau}{18\pi^2 T^2}(1 - \pi T\tau), \\ \Omega_3^{(4)}(k) = {} & -\frac{i}{\tau} + \frac{ik^2}{3\pi T} - \frac{ik^4\tau}{9\pi^2 T^2}(-1 + \pi T\tau). \end{aligned} \quad (20)$$

Here, $\Omega_3^{(4)}(k)$ is a purely imaginary, damped mode, while $\Omega_{1,2}^{(4)}(k)$ modes are propagating modes with some attenuation. For order 10 expansion, the hydroseries takes the following form:

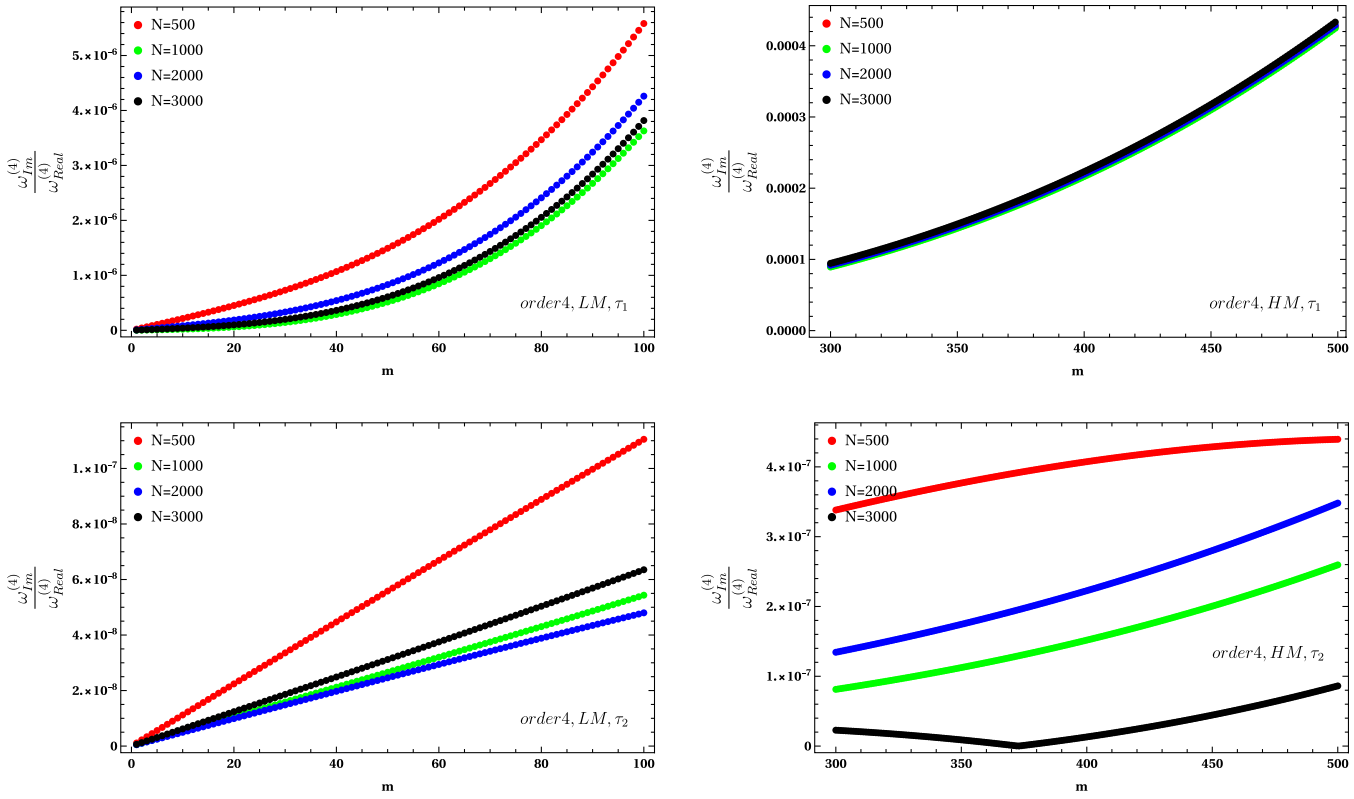

FIG. 1. The ratio $\omega^{(4)}_{\mathrm{Im}}/\omega^{(4)}_{\mathrm{Real}}$ for various particle numbers in the fourth-order series expansion. The top plots display the results for τ_1, and the bottom plots show the results for τ_2. The left column corresponds to LM bins, and the right column represents HM bins.

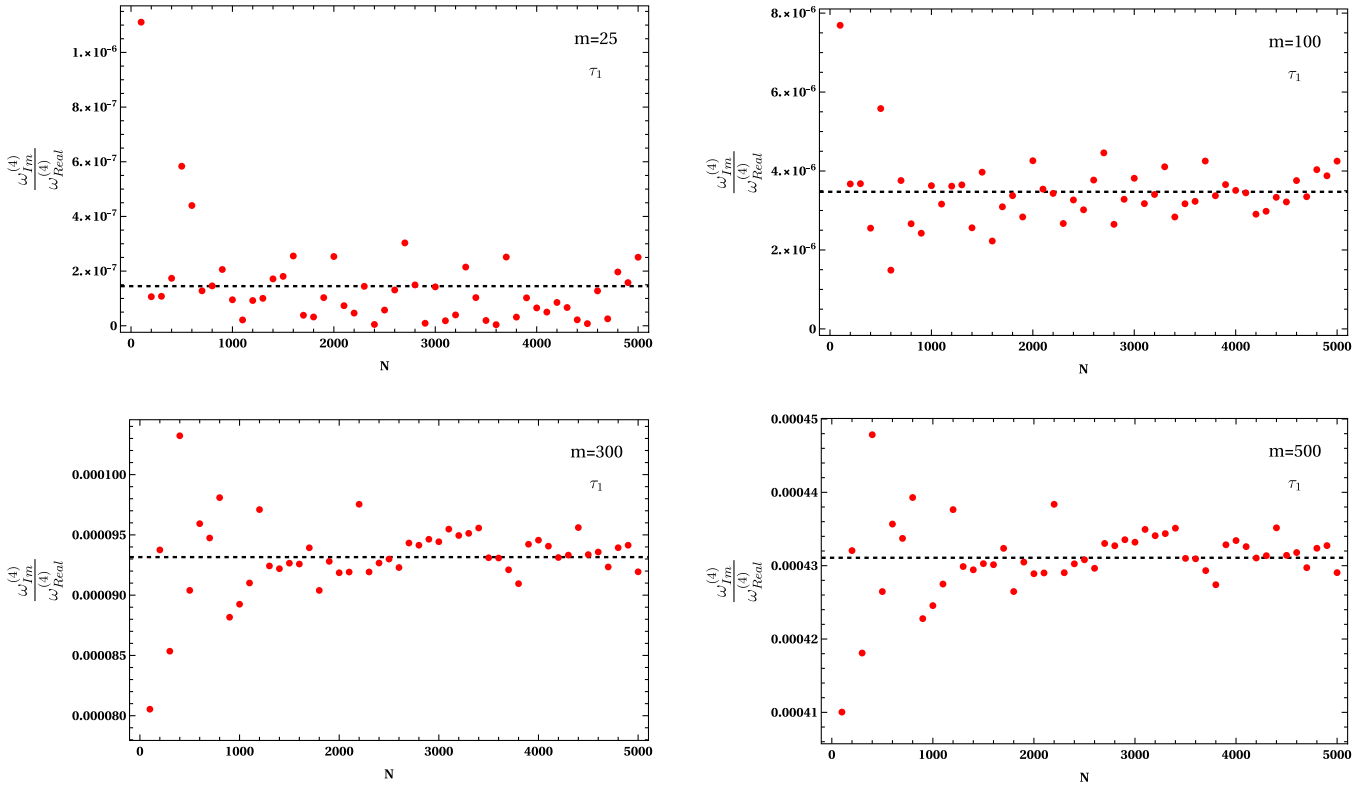

FIG. 2. Plot of $\omega^{(4)}_{\mathrm{Im}}/\omega^{(4)}_{\mathrm{Real}}$ in terms of particle numbers for specific momentum bins. The results are shown for the τ_1 case in the fourth-order expansion, utilizing Eq. (16).

$$\Omega^{(10)}_{1,2}(k) = \pm\Bigg(\frac{k}{\sqrt{3}} + \frac{k^3}{24\sqrt{3}\pi^2T^2}(-1+4\pi T\tau) - \frac{k^5(8\pi\tau T(2\pi\tau T(4\pi\tau T-9)+3)+1)}{1152\sqrt{3}\pi^4T^4}$$
$$+ \frac{k^7(4\pi\tau T(4\pi\tau T(8\pi\tau T(\pi\tau T-5)(4\pi\tau T-5)-25)-5)-1)}{27648\sqrt{3}\pi^6T^6}$$
$$- \frac{k^9(16\pi\tau T(2\pi\tau T(4\pi\tau T(2\pi\tau T(8\pi\tau T(2\pi\tau T-7)(4\pi\tau T-35)-1225)+245)+49)+7)+5)}{2654208\sqrt{3}\pi^8T^8}\Bigg),$$
$$-\frac{ik^2}{6\pi T} - \frac{ik^4\tau}{18\pi^2T^2}(1-\pi T\tau) - \frac{ik^6\tau^2(\pi\tau T(\pi\tau T-4)+2)}{54\pi^3T^3} + \frac{ik^8\tau^3(\pi\tau T(\pi\tau T(\pi\tau T-9)+15)-5)}{162\pi^4T^4}$$
$$- \frac{ik^{10}\tau^4(\pi\tau T(\pi\tau T-2)(\pi\tau T(\pi\tau T-14)+28)+14)}{486\pi^5T^5},$$

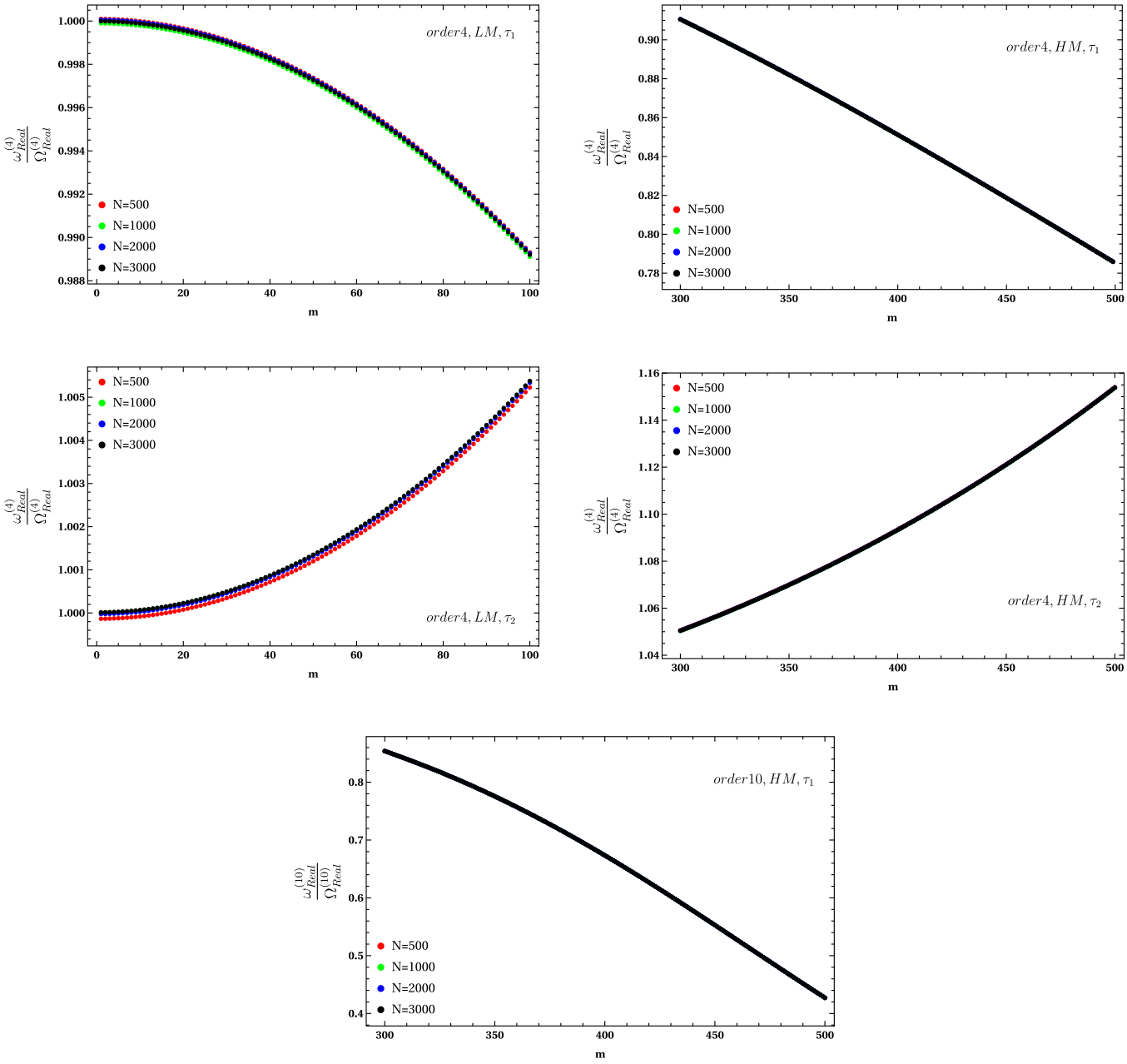

FIG. 3. The ratio $\omega^{(4)}_{\text{Real}}/\Omega^{(4)}_{\text{Real}}$ for various particle numbers. The top row and the very bottom plot correspond to τ_1 and the middle plots belong to the order 4 expansion calculated with τ_2.

$$\Omega_3^{(10)}(k) = -\frac{i}{\tau} + \frac{ik^2}{3\pi T} - \frac{ik^4\tau}{9\pi^2T^2}(-1+\pi T\tau) + \frac{ik^6\tau^2(\pi\tau T(\pi\tau T-4)+2)}{27\pi^3T^3} + \frac{ik^8\tau^3(5-\pi\tau T(\pi\tau T(\pi\tau T-9)+15))}{81\pi^4T^4} + \frac{ik^{10}\tau^4(\pi\tau T(\pi\tau T-2)(\pi\tau T(\pi\tau T-14)+28)+14)}{243\pi^5T^5}. \tag{21}$$

After setting all the stages, we are now exploring different cases. In Fig. 1, we illustrate the average ratio $\omega_{\mathrm{Im}}^{(4)}/\omega_{\mathrm{Real}}^{(4)}$ for various particle numbers in both LM and HM bins, with $\tau_1 = (2-\ln 2)/(2\pi T)$ and $\tau_2 = 0.1/(2\pi T)$. The top panel corresponds to τ_1, while the bottom panel represents τ_2. Also, the left column displays the LM results, and the right column shows the HM results. To calculate this ratio, we generated roots based on Eq. (16) for LM bins with $m = (1, \ldots, 100)$ and HM bins with $m = (300, \ldots, 500)$. We then extracted the imaginary and real parts and fitted them to the optimal Gaussian distribution as shown in Eq. (19). Afterward, we divided the

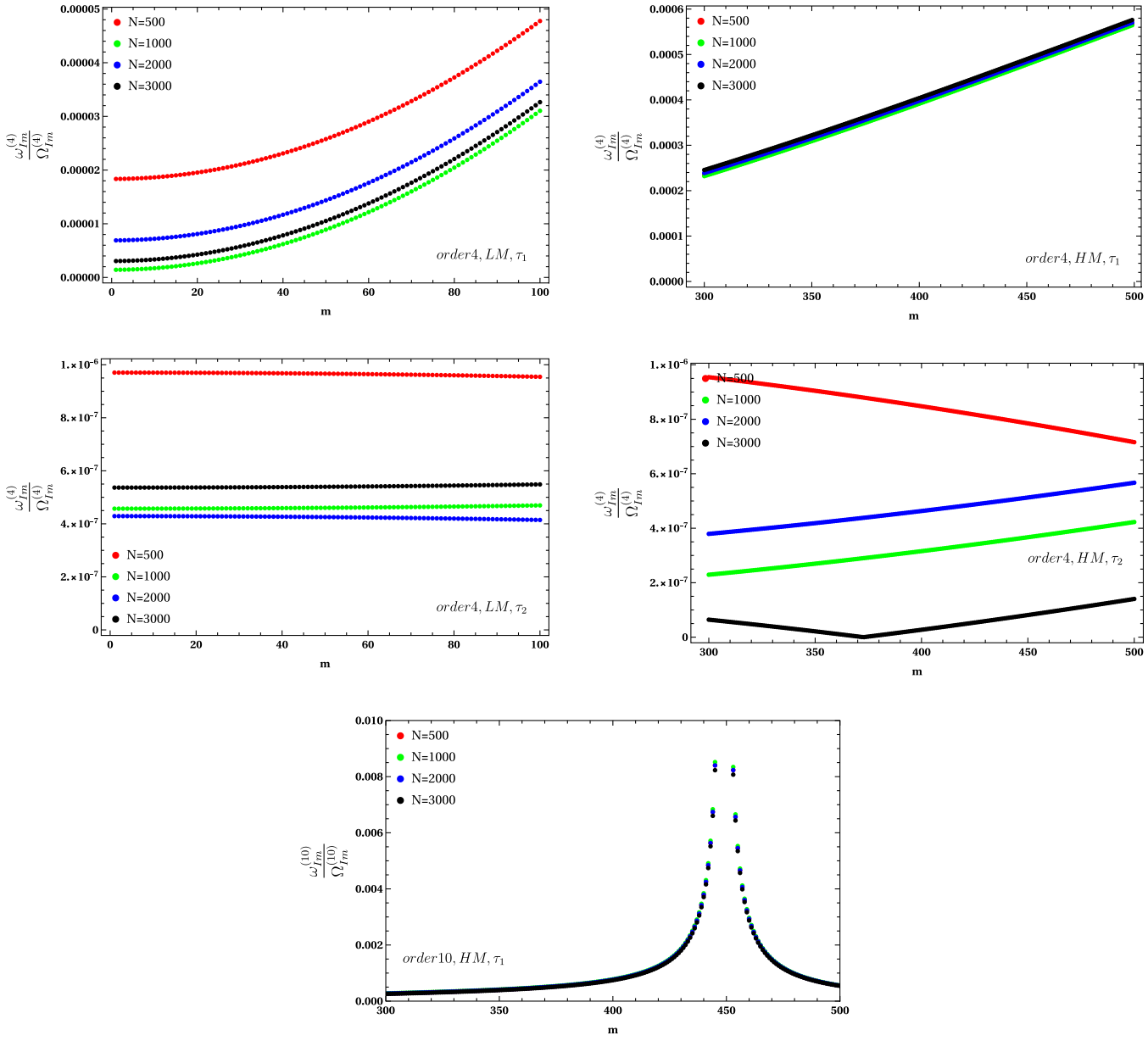

FIG. 4. The ratio $\omega_{\mathrm{Im}}^{(4)}/\Omega_{\mathrm{Im}}^{(4)}$ for various particle numbers. The top row and the very bottom plot correspond to τ_1 and the middle plots belong to the order 4 expansion calculated with τ_2.

mean values of each part and organized them according to the value of "m" for different particle numbers. The results indicate a mild increase with respect to momentum, while the number of particles has a negligible impact. For τ_1, there is a significant difference between the LM and HM results. In contrast, for τ_2, the results for both LM and HM fall within the same range. We shall elaborate on this fact in the next few lines.

From Fig. 1, we observe an oscillatory pattern in the ratio $\omega^{(4)}_{\mathrm{Im}}/\omega^{(4)}_{\mathrm{Real}}$ as a function of N. In Fig. 2, we present this ratio across the full range of particle numbers for specific momentum bins at τ_1. The horizontal dashed line represents the average value of this ratio. The results of τ_2 behave similarly.

In Fig. 3, we examine the ratio between the real parts of the randomly generated modes, as described in Eq. (16), and their counterparts in the hydrodynamic modes, presented in Eq. (20), for various particle numbers in either LM or HM bins. Each plot represents a specific case of τ with the HM or LM bin, as indicated. In the top row for τ_1, we see that as momentum increases, the ratio $\omega^{(4)}_{\mathrm{Real}}/\Omega^{(4)}_{\mathrm{Real}}$ decreases and even higher-order expansions yield smaller values, as shown in the very bottom plot. The results for τ_2 in the middle row demonstrate that going to HM yields larger values, and the expansion order 10 gives no sizable difference with the order 4. For τ_1, this ratio is less than one, while for τ_2, the ratio is greater than one. Comparing the very top right panel with the very bottom one in Fig. 3 has shown that at HM our ability to predict propagating modes diminishes because different orders produce different results for τ_1. Its message is that we can no longer rely on ansatz (14) in this region. This is because, intuitively, at high momenta, we pass the radius of the convergence of the sound hydroseries which invalidates the use of ansatz (14). More interestingly, for the MIS model, the regions of convergence and analyticity are identical [30], and moving beyond convergence means entering a nonanalytic region. This fact does not matter to thermal fluctuations and only the momentum running pushes us into the nonanalytic, divergence zone. The size of this region depends on τ/T. For instance, when $\tau = \tau_1$ the points beyond $m \gtrapprox 300$ lie within the nonanalytic zone, whereas for $\tau = \tau_2$ the points beyond $m \gtrapprox 1000$ are inside the nonanalytic zone. That is why we do not include the "order 10, HM, τ_2 part in Fig. 3.

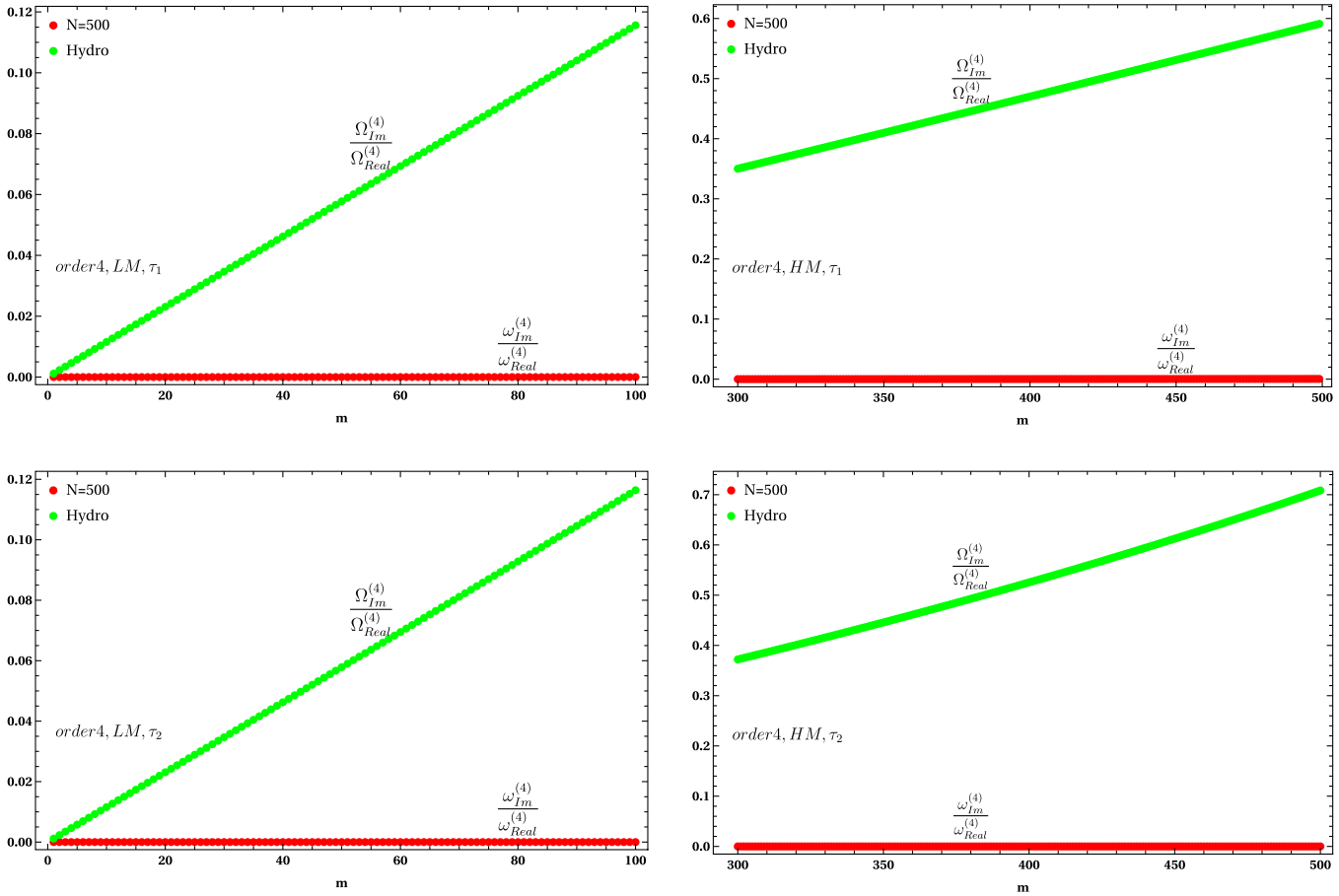

FIG. 5. Comparing the imaginary to real parts for the hydromodes and the randomly generated modes. The top (bottom) row corresponds to τ_1 (τ_2). The left (right) panels address the LM (HM) results.

In Fig. 4, we display the findings for the imaginary components. In comparison to the real components, the values are considerably smaller. At τ_1, the results exhibit a greater sensitivity to the momentum bin, whereas this sensitivity is smaller in the τ_2 plots. Furthermore, for the tenth-order expansion at τ_1 in the HM bin, there is a noticeable bump around a certain value, which arises from the zero value of $\Omega_{\mathrm{Im}}^{(10)}$.

Another intriguing aspect to consider is the comparison between the ratio of imaginary to real parts for both randomly generated modes and hydrodynamic modes. This comparison is depicted in Fig. 5. The top row corresponds to τ_1, while the bottom row represents τ_2. Similarly, the left plots show LM results and the right plots display HM results. The ratio for hydrodynamic modes is consistently greater than that for random modes. For other scenarios, such as the tenth-order expansion, the results do not exhibit significant differences from those shown in Fig. 5.

As mentioned above, moving to the HM region would lose our predictive power, since the structure of solutions alters in the HM due to the presence of branch cuts [27,30]. This phenomenon is observed in Fig. 6, where we illustrate the evolution of the real and imaginary parts of the hydrodynamic modes in both of the LM and HM regions for τ_1 in the top row and τ_2 in the bottom row. The red (blue) color traces the path of the fourth- (tenth-) order series corresponding to Eqs. (20) and (21), respectively. In the LM region, the order of expansion does not significantly affect the results. However, in the HM region, the series order does impact the real and imaginary parts, particularly for τ_1. This is because, around $m \sim 300$, the solutions $\omega(k)$ transit from exhibiting two propagating and one dispersive mode to three propagating modes, a change attributed to the alteration in branch cuts. For τ_2, this shift point moves approximately to $m \sim 1000$, where the modes undergo a similar change. Since the latter point is too distant to be displayed in Fig. 6, the colors in the bottom plots are so close to each other.

Concluding this discussion should emphasize again that convergence and analyticity are somewhat distinct concepts. In works such as [19,20] it was argued that deterministic transport models generally have nonanalytic cuts in the IR which do not impact the convergence of the Knudsen series. In [31,32], on the other hand, perturbative fluctuations are shown to introduce both nonanalyticity and lack of convergence cascading from the UV to the IR ("long-time tails"). As argued in the Introduction, soft

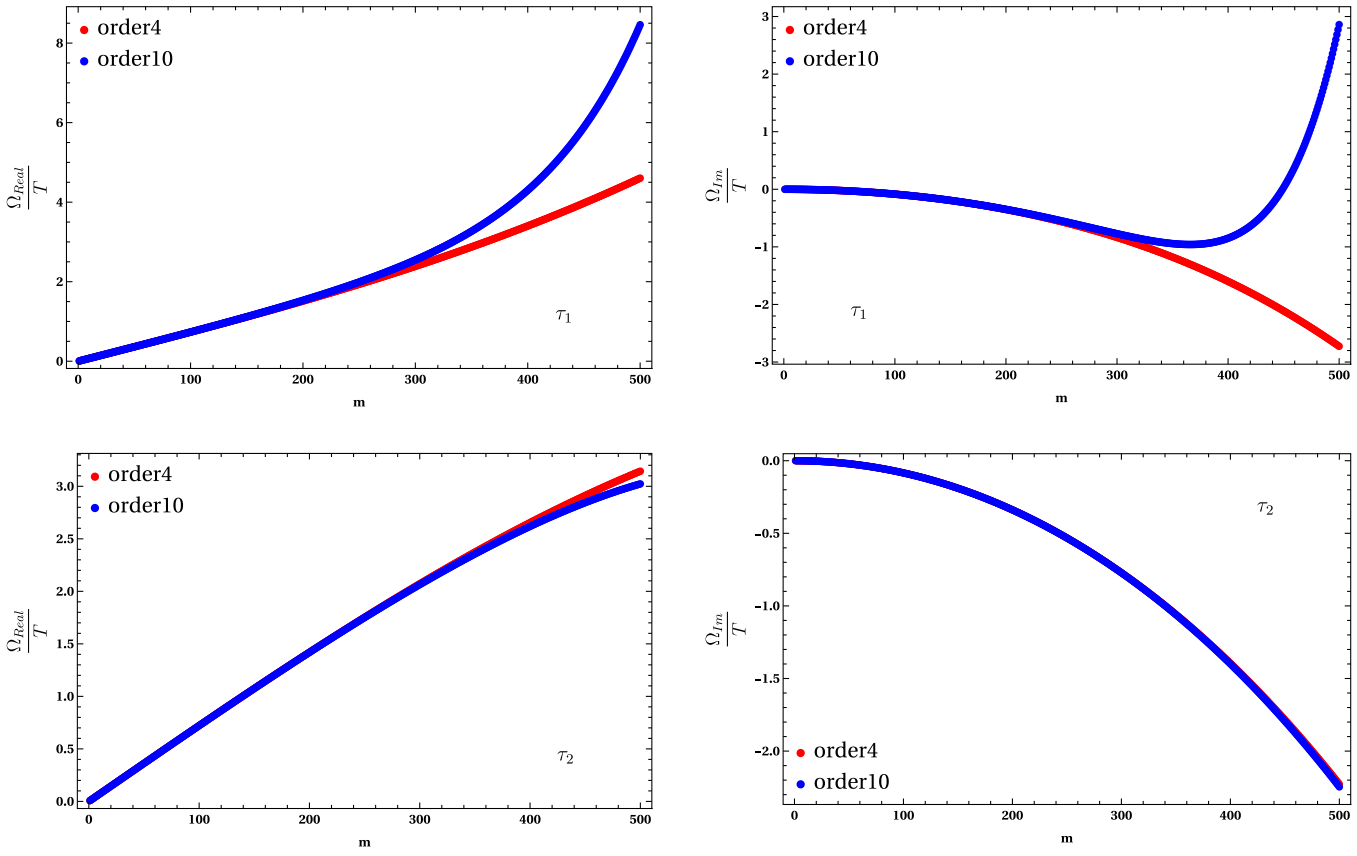

FIG. 6. The evolution of the real and imaginary parts of the hydrodynamic modes in terms of momentum bin. The top row displays the results for τ_1, and the bottom row shows the results for τ_2. Different colors correspond to different orders of expansion as provided in Eqs. (20) and (21).

nonanalyticity is in principle indistinguishable from hydrodynamic modes when fluctuations are included, so our random coefficients include any soft modes in the $\langle T_{\alpha\beta}T_{\gamma\mu}\rangle$ correlator, which are by definition called hydrodynamic modes. Our random coefficients ansatz is based on thermal fluctuations being treated as "large" with respect to the Knudsen series, so the regime of validity is different from that discussed in [31,32]. However, the correlation between convergence and analyticity as argued in [30] suggests that provided convergence holds analyticity becomes a moot point since any nonhydrodynamic modes can be accounted for by fluctuating coefficients. In this case, the effect of fluctuations on the distribution of imaginary to real poles can alter the impact of long-lived hydrodynamic modes considerably with respect to perturbative expectations.

V. CONCLUSION

As can be seen, the introduction of fluctuations consistently lowers the ratio of imaginary to real parts of the roots at all ω/T and makes the distribution of the roots "scale invariant" with respect to ω/T. Since, as far as we know, the type of series shown here has not been studied beyond numerics (exact mathematical results [12–14,33] concern polynomials where all coefficients are of the same order), we are not aware of a mathematical justification for this, beyond a naive appeal to the Kac formula (where the fraction of real roots goes to zero but the probability of finding at least a real root goes to unitary as order increases).

The calculations here are certainly naive, only involving sound and shear modes rather than vorticity. Nevertheless, if they capture the essential physics, the results are remarkable. They provide evidence for the conjecture made in [7,10,34] that hydrodynamic behavior does not necessarily go down with the number of constituents: Because the background fluctuates, and because the condition for long-range propagation is a delicate correlation of all coefficients in the dispersion relation, it might be that fluctuations allow asymptotic propagation to be "selected out."

There is certainly quite a lot of work to be done in this direction. It will be interesting to see if the results are maintained as the order of the polynomial goes to infinity, connected to studied by other methods in [35]. Likewise, it will be interesting to see the probability structure of the analytical features (critical points, real vs imaginary roots) of fluctuating polynomials and to relate this to the gap problem [11,19–21]. It would also be interesting to see whether dispersion relations with fluctuating coefficients can be used to quantitatively model collective systems with few degrees of freedom obtainable in more controlled laboratory conditions, such as [4,5].

The larger point here is that we do not know exactly how the hydrodynamic limit is approached when both the microscopic scale and the mean free path are varied [3]. It is commonly assumed that even in the strongly coupled limit one gets closer to ideal hydrodynamics when one increases the number of degrees of freedom. This is a reasonable assumption but there is no solid evidence for it and in fact the evidence in [1,4,5] pushes us to question it. The indications, discussed here, that adding background fluctuations to hydrodynamic dispersion relations nontrivially changes long-distance propagation could therefore profoundly affect our understanding of the onset of collectivity in small systems.

ACKNOWLEDGMENTS

G. T. acknowledges support from Bolsa de produtividade CNPQ 305731/2023-8 and Bolsa de pesquisa FAPESP 2023/06278-2. We sincerely thank Saso Grozdanov for discussions and suggestions.

APPENDIX: RANDOM POLYNOMIALS: A BRIEF REVIEW

A random function is defined as a probability measure on the space of functions that map from a set of parameters [12]. By establishing a basis $(f_0(t), f_1(t), \ldots, f_N(t))$ (which does not necessarily have to be orthonormal) and selecting a random complex vector, such as $X = (x_0, x_1, \ldots, x_N)$, we can construct a random function $f(t)$ as follows:

$$f: T \to \mathbb{R}, \qquad f(t) = \sum_{i=0}^{N} x_i f_i(t). \tag{A1}$$

This random function is characterized by the probability distribution that describes the likelihood of each event

$$\mathbb{P} = p(x_0, x_1, \ldots, x_N) dx_0 dx_1 \ldots dx_N, \quad x_i \in (\bar{x}_i, \bar{x}_i + dx_i), \tag{A2}$$

where the probabilities are normalized to sum to one,

$$\int_{\text{All X}} p(x_0, x_1, \ldots, x_N) dx_0 dx_1 \ldots dx_N = 1. \tag{A3}$$

The elements of the set X can be generated from various random distributions, including uniform and Gaussian distributions. When using a uniform distribution, the elements are generated randomly and independently without any correlation. In contrast, other distributions, such as the Gaussian distribution, produce numbers that are correlated with each other.

The fundamental theorem of algebra tells us that, for any polynomial $f(t)$ of degree n with coefficients in $\mathbb{C}$, there exist n roots, counting multiplicity, such that $f(t) = 0$. This theorem leads to several intriguing questions:

(1) Given the distribution of coefficients X, what is the distribution of the roots of $f(t) = 0$? More specifically, what can we say about the distribution of the

absolute values of the roots and their phases, assuming a certain distribution of coefficients?.
(2) How many real roots can we expect for $f(t) = 0$?.
(3) What is the distribution of the real roots of $f(t) = 0$?.

These questions have sparked extensive research in the field of pure mathematics [12–14,33]. For lower-degree polynomials, it is relatively straightforward to compute probabilities using closed-form solutions. However, the lack of general analytical solutions makes the task significantly more complex for higher-degree polynomials (specifically, those of degree 5 or greater).

The Kac-Rice formula provides a general solution to this problem. Consider a random function $f(t)$, as defined in Eq. (A1), with a distribution given by

$$p_{f(t)}(X)dX = p_{f(t)}(x_0, \ldots, x_N)dx_0 \ldots dx_N, \tag{A4}$$

where the density $p_{f(t)}(X)$ is continuous at zero, and the coefficients X are drawn from the set of real numbers. The expected number of real roots, denoted by $\hat{Z}(f, T)$, can be expressed as

$$\hat{Z}(f, T) = \sum_{k=0}^{N} k\mathbb{P}_R(k), \tag{A5}$$

where $\mathbb{P}_R(k)$ is the probability of having k real roots. The Kac-Rice formula offers an alternative expression

$$\begin{aligned} \hat{Z}(f, T) &= \int_T dt C(t), \\ C(t) &= \mathbf{E}(f'(t)|f(t) = 0)p_{f(t)}(0), \end{aligned} \tag{A6}$$

where $\mathbf{E}(f'(t)|f(t) = 0)$ is the conditional expectation of the derivative $f'(t) = df(t)/dt$ given that $f(t) = 0$, and the integral is taken over the range of the random variable "t." The conditional expectation is defined as

$$\begin{aligned} \mathbf{E}(f'(t)|f(t) = 0) &= \int_{\mathbb{R}} dy|y|q_t(y), \\ q_t(y) &= \frac{p_t(0, y)}{p_{f(t)}(0)}, \\ p_{f(t)}(X) &= \int_{\mathbb{R}} dy p_t(X, y). \end{aligned} \tag{A7}$$

Equations (A6) and (A7) can be seen as the continuous analogs to the discrete formulation in Eq. (A5).

If we assume a Gaussian distribution for $f(t)$, the analysis becomes significantly simpler. The random vector $(f'(t), f(t)) \in \mathbb{R}^2$ follows a Gaussian distribution, which is characterized by its covariance matrix

$$C_t = \begin{pmatrix} a_t & b_t \\ b_t & c_t \end{pmatrix}, \tag{A8}$$

where

$$\begin{aligned} a_t &= \mathbf{E}(f'(t)^2) = \left.\frac{\partial^2 K(s,t)}{\partial s \partial t}\right|_{s=t}, \\ b_t &= \mathbf{E}(f(t)f'(t)) = \left.\frac{\partial K(s,t)}{\partial t}\right|_{s=t}, \\ c_t &= \mathbf{E}(f(t)^2) = K(t,t), \end{aligned} \tag{A9}$$

and $\mathbf{E}(.)$ denotes the expectation of the term within the parentheses. Here, $K(s,t) = \mathbf{E}(f(s)f(t))$ is the covariance kernel. Defining $\vec{F} \equiv (y, x) = (f'(t), f(t))$, the joint distribution is given by

$$\Gamma_{C_t} dxdy = \frac{1}{2\pi\sqrt{\Delta_t}} e^{-\frac{\vec{F}^T \cdot C_t \cdot \vec{F}}{2\Delta_t}} dxdy, \tag{A10}$$

with $\Delta_t = \det(C_t) = a_t c_t - b_t^2$. Substituting this joint distribution into Eq. (A6) and performing some calculations, we obtain [12]

$$\hat{Z}(f, T) = \frac{1}{\pi}\int_T dt \rho_t, \tag{A11}$$

where

$$\rho_t = \frac{\sqrt{\Delta_t}}{a_t} = \sqrt{\left.\frac{\partial^2 \ln K(s,t)}{\partial s \partial t}\right|_{s=t}}. \tag{A12}$$

For example, consider the degree N polynomial

$$f_N(t) = \sum_{k=0}^{N} x_k t^k, \tag{A13}$$

with a uniform distribution such that $\langle x_i x_j \rangle = \delta_{ij}$. The covariance kernel for this polynomial is

$$K_N(s,t) = \mathbf{E}(f(s)f(t)) = \frac{1 - (st)^{N+1}}{1 - st}, \tag{A14}$$

and Eq. (A11) yields

$$\hat{Z}(f_N, T) = \frac{4}{\pi}\int_1^{\infty} dt \sqrt{F_N(t)}, \tag{A15}$$

where

$$F_N(t) = \frac{1}{(1-t^2)^2} - \frac{(N+1)^2 t^{2N}}{(1-t^{2N+2})^2}. \tag{A16}$$

For $N = 2$, this gives $\hat{Z}(f_2) \simeq 1.279$, which is close to 1.256. For $N = 3$, it gives $\hat{Z}(f_3) \simeq 1.492$, which agrees well with numerical computations. For higher values of N, Eq. (A15) provides results close to those obtained numerically. It has been argued that the large N

asymptotic behavior of the expected number of real roots in a random real function with a uniform distribution is given by [13]

$$\hat{Z}(f_N)|_{N\to\infty} \simeq \frac{2\ln(eN)}{\pi}. \tag{A17}$$

It is important to note that Eq. (A11) can be applied to many random functions with different distributions, provided that the covariance kernel can be derived analytically. However, the Kac-Rice formula does not provide information about the distribution of real roots or the distribution of roots in general.

[1] J. L. Nagle and W. A. Zajc, Small system collectivity in relativistic hadronic and nuclear collisions, Annu. Rev. Nucl. Part. Sci. **68**, 211 (2018).

[2] P. Kovtun, Lectures on hydrodynamic fluctuations in relativistic theories, J. Phys. A **45**, 473001 (2012).

[3] D. Montenegro, R. Ryblewski, and G. Torrieri, Relativistic fluid dynamics and its extensions as an effective field theory, Acta Phys. Pol. B **50**, 1275 (2019).

[4] S. Brandstetter *et al.*, Emergent hydrodynamic behaviour of few strongly interacting fermions, arXiv:2308.09699.

[5] C. Güttler, I. von Borstel, R. Schräpler, and J. Blum, Granular convection and the Brazil nut effect in reduced gravity, Phys. Rev. E **87**, 044201 (2013).

[6] P. Kovtun, G. D. Moore, and P. Romatschke, The stickiness of sound: An absolute lower limit on viscosity and the breakdown of second order relativistic hydrodynamics, Phys. Rev. D **84**, 025006 (2011).

[7] T. Dore, L. Gavassino, D. Montenegro, M. Shokri, and G. Torrieri, Fluctuating relativistic dissipative hydrodynamics as a gauge theory, Ann. Phys. (Amsterdam) **442**, 168902 (2022).

[8] G. Torrieri, Emergent symmetries of relativistic fluid dynamics from local ergodicity, Phys. Rev. D **109**, L051903 (2024).

[9] V. Khachatryan *et al.* (CMS Collaboration), Evidence for collectivity in pp collisions at the LHC, Phys. Lett. B **765**, 193 (2017).

[10] G. Torrieri, The functional generalization of the Boltzmann-Vlasov equation and its Gauge-like symmetry, SciPost Phys. **16**, 070 (2024).

[11] G. D. Moore, Stress-stress correlator in ϕ^4 theory: Poles or a cut?, J. High Energy Phys. 05 (2018) 084.

[12] L. I. Nicolaescu, Counting zeroes of random functions, Am. Math. Mon. **130**, 625 (2022).

[13] H. Nguyen, O. Nguyen, and V. Vu, On the number of real roots of random polynomials, Commun. Contemp. Math. **18**, 1550052 (2016).

[14] M. Kac, On the average number of real roots of a random algebraic equation, Bull. Am. Math. Soc. **49**, 314 (1943).

[15] S. Grozdanov, Bounds on transport from univalence and pole-skipping, Phys. Rev. Lett. **126**, 051601 (2021).

[16] S. Grozdanov, P. K. Kovtun, A. O. Starinets, and P. Tadić, Convergence of the gradient expansion in hydrodynamics, Phys. Rev. Lett. **122**, 251601 (2019).

[17] S. Grozdanov, P. K. Kovtun, A. O. Starinets, and P. Tadić, The complex life of hydrodynamic modes, J. High Energy Phys. 11 (2019) 097.

[18] J. Hickman and Y. Mishin, Temperature fluctuations in canonical systems: Insights from molecular dynamics simulations, Phys. Rev. B **94**, 184311 (2016).

[19] L. Gavassino, Gapless non-hydrodynamic modes in relativistic kinetic theory, arXiv:2404.12327.

[20] G. S. Rocha, I. Danhoni, K. Ingles, G. S. Denicol, and J. Noronha, Branch-cut in the shear-stress response function of massless $\lambda\varphi^4$ with Boltzmann statistics, arXiv:2404.04679.

[21] R. Gangadharan and V. Roy, The convergence problem of gradient expansion in the relaxation time approximation, arXiv:2405.10846.

[22] M. McNelis and U. Heinz, Hydrodynamic generators in relativistic kinetic theory, Phys. Rev. C **101**, 054901 (2020).

[23] G. S. Denicol, H. Niemi, E. Molnar, and D. H. Rischke, Derivation of transient relativistic fluid dynamics from the Boltzmann equation, Phys. Rev. D **85**, 114047 (2012); **91**, 039902(E) (2015).

[24] S. Endlich, A. Nicolis, R. Rattazzi, and J. Wang, The quantum mechanics of perfect fluids, J. High Energy Phys. 04 (2011) 102.

[25] G. Soares Rocha, L. Gavassino, and N. Mullins, Modeling stochastic fluctuations in relativistic kinetic theory, Phys. Rev. D **110**, 016020 (2024).

[26] R. F. Fox and G. E. Uhlenbeck, Contributions to nonequilibrium thermodynamics. II. Fluctuation theory for the Boltzmann equation, Phys. Fluids **13**, 2881 (1970).

[27] S. Grozdanov, A. Lucas, and N. Poovuttikul, Holography and hydrodynamics with weakly broken symmetries, Phys. Rev. D **99**, 086012 (2019).

[28] R. Baier, P. Romatschke, D. T. Son, A. O. Starinets, and M. A. Stephanov, Relativistic viscous hydrodynamics, conformal invariance, and holography, J. High Energy Phys. 04 (2008) 100.

[29] L. Landau and E. Lifshitz, *Statistical Physics* (Elsevier Science, New York, 2013), Vol. 5.

[30] R. Heydari and F. Taghinavaz, Local univalence versus stability and causality in hydrodynamic models, arXiv:2404.14091.

[31] L. V. Delacretaz, Heavy operators and hydrodynamic tails, SciPost Phys. **9**, 034 (2020).

[32] S. Grozdanov, T. Lemut, J. Pelaič, and A. Soloviev, Analytic structure of diffusive correlation functions, arXiv:2407.13550.

[33] C. Berzin, A. Latour, and J. León, Kac-rice formula: A contemporary overview of the main results and applications, arXiv:2205.08742.

[34] D. Zubarev, *Nonequilibrium Statistical Thermodynamics* (Springer US, 1974).

[35] S. Grozdanov (private communication).